Investigating the Corrosion Behavior of Corrosion-Resistant Alloys in Solutions Containing Dilute Fluoride Ions

*J.D. Henderson,[*] S. Ramamurthy,[**] F.P. Filice,[*] M.C. Biesinger,[***] D.W. Shoesmith,[***] G.B. McGarvey,[***] and J.J. Noël[‡,***]*

The ability of fluoride ions, in trace concentrations, to promote film instability and transpassive dissolution was shown for several corrosion-resistant alloys. While the addition of fluoride ion was found to decrease the transpassive dissolution potential by approximately 0.1 V, the decrease was particularly pronounced in mildly acidic media (pH 5). Results suggest that the decreased potential range of stability for the heavily-relied-upon Cr(III)-rich oxide film is a concern in the presence of oxidizing impurities, which may push the corrosion potentials toward the transpassive region. The decreased potential range of passive film stability was observed using both dynamic and static polarization experiments and was supported by solution and surface analyses.

KEY WORDS: chloride, fluoride, Ni-Cr-Mo alloy, stainless steel, transpassivity

INTRODUCTION

The role of halide anions, particularly chloride (Cl^-), in corrosion processes has been extensively discussed in the literature.[1-4] However, information regarding corrosion induced by the presence of fluoride ions (F^-) is much less abundant, especially for corrosion in conditions other than concentrated hydrofluoric acid (HF). Research on corrosion-resistant alloys exposed to concentrated HF is required by industries such as the petrochemical industry, which uses high concentrations of HF in alkylation units. These units, which are usually built of carbon steel, operate under extremely acidic conditions.[5] Failure of these structures becomes possible when the HF concentration drops or the temperature is increased, resulting in increased corrosion rates.[5] To minimize damage, acid concentrations are kept high in HF alkylation units.

Recent research has focused on determining optimal Ni-based alloy compositions to improve corrosion resistance and mechanical properties in concentrated HF solutions. Li, et al., demonstrated the importance of the formation of a Mo-rich surface layer on the corrosion resistance of Ni alloys in 5.2 M HF.[6] Although the ability to form a Mo-rich surface layer improved the corrosion resistance, further improvements could be realized with Cu additions. With alloying additions of 2 wt% Cu, the Mo oxide film previously observed was replaced by a segregated Cu-rich surface layer,[7] yielding an increase in corrosion resistance relative to alloys containing no Cu. Among the commercially available Ni alloys, Hastelloy C2000[†] has been of particular interest in this regard due to its Cu content.[8] Unfortunately, the information reported in these studies is not immediately applicable to environments containing low F^- concentrations and/or pH values near neutral, e.g., pH 5 to pH 9.

Research involving the corrosion behavior of corrosion-resistant alloys in low or trace concentrations of F^- is sparse, with the most relevant studies conducted on dental materials and materials used in proton exchange membrane fuel cell (PEMFC) applications.[9-13] However, the materials used in dental applications are commonly Ti-based due to their biocompatibility; therefore, these studies, although instructive, are not useful for large-scale material applications where the use of Ti-based alloys is not appropriate.

Accordingly, the petrochemical industry lacks data regarding the corrosion behavior of corrosion-resistant alloys exposed to trace F^- environments. However, there are several industrial processes that may introduce low or trace concentrations of F^- during refinery processing. Commonly used cleaning solvents, acidizing procedures used to increase the productivity of reservoirs,[14] and the reprocessing of F^--containing refinery streams can act as sources of F^- contamination throughout refinery operations. Therefore, determining the extent of interaction between F^- and the materials found within the refinery is essential to ensure safe operation.

As described, most previous work has focused on concentrated F^- environments, and little is known about the corrosion of corrosion-resistant alloys in dilute F^- solutions (concentrations up to 5,000 ppm) and at increased temperatures (80°C to 120°C) and pH values close to neutral. Thus,

Submitted for publication: November 23, 2020. Revised and accepted: February 16, 2021. Preprint available online: February 16, 2021, https://doi.org/10.5006/3736.
‡ Corresponding author. E-mail: jjnoel@uwo.ca.
* Department of Chemistry, Western University, London, Ontario, N6A 5B7, Canada.
** Surface Science Western, Western University, London, Ontario, N6G 0J3, Canada.
*** Sarnia Technology Applications & Research, Imperial Oil, Sarnia, Ontario, N7T 8C8, Canada.
† Trade name.

ISSN 0010-9312 (print), 1938-159X (online)

the motivation for this project was the development of an understanding of the effects of F^- on a variety of commercially available alloys that could be appropriate in such an environment. In addition, experiments were conducted in the presence of Cl^-, a common co-contaminant in refinery environments.[14] Electrochemical investigations in the form of open-circuit and polarization experiments were conducted in relevant environments. Complementary surface and solution analyses were performed following potentiostatic polarization experiments to understand changes in film composition and structure as a function of the applied potential and the solution environment.

EXPERIMENTAL PROCEDURES

2.1 | Material Preparation

Both Ni- and Fe-based alloys were received as mill-annealed sheets. Ni alloys were provided by Haynes International† (Kokomo, IN, USA), while Fe-based alloys were purchased from McMaster-Carr† (Elmhurst, IL, USA). The nominal compositions, reported in Table 1, are in accordance with ASTM B462 and A240.

Coupons were cut and machined to the desired size from the mill-annealed sheets. Prior to electrochemical measurements, coupons were ground with a series of wet SiC papers (P600–P1200) to remove any damage incurred during the machining process and to create a reproducible surface. Coupons intended for subsequent surface analysis were further ground until a final step using P4000 SiC paper to minimize surface topography. Prepared coupons were sonicated in a 1:1 mixture of deionized (DI) water (18.2 $M\Omega \cdot cm^2$) and ethanol for 30 s, rinsed in DI water, and then dried in a stream of argon (Ar) gas. In all cases, the coupons were prepared immediately before each experiment.

Solutions were prepared using reagent grade Na_2SO_4 (Fisher Scientific†), KF (VWR International†), NaCl (Caledon Laboratory Chemicals†), and DI water (Thermo Scientific Barnstead† Nanopure†). The pH of each solution was adjusted using solutions of H_2SO_4 (Caledon Laboratory Chemicals) and NaOH (Fisher Scientific). To ensure adequate solution conductivity during all experiments, a supporting electrolyte (0.1 M Na_2SO_4) was used, with the specified concentrations of F^- and Cl^- added to this solution.

2.2 | Electrochemical Measurements

Electrochemical experiments were conducted in a polytetrafluoroethylene (PTFE) electrochemical cell, fabricated in house, as shown in Figure 1(a). Two lids were constructed for use with the cell, depending on experimental needs. The first lid was designed with three inlets for electrode connections, as depicted in Figure 1(b). A second lid was designed with eight inlets for electrode connections, making the simultaneous measurement of up to six working electrodes (WE) possible, as depicted in Figure 1(c). A saturated Ag/AgCl electrode (0.199 V_{NHE} [normal hydrogen electrode]) and a platinum coil were used as the reference electrode (RE) and counter electrode (CE), respectively. Both lids had inlet and outlet fittings used for solution sparging. All connections were wrapped in PTFE tape to ensure a secure, airtight fit. Once assembled, the cell was secured in a custom-machined clamp to ensure no movement of fittings during heating or Ar sparging. Temperature control was achieved using a custom-built heating reservoir adapted for use with an external isothermal water circulator. The fully

Table 1. *Nominal Compositions of Studied Alloys in wt%*[(A)]

Alloy	Ni	Cr	Mo	Fe	W	Cu	Nb*	Co	Mn	Ti	Al	V	N	Si	C
SS316L	14^M	18^M	3^M	Bal.	—	—	—	—	2	—	—	—		0.75	0.03
SS2205	6.5^M	23^M	3.5^M	Bal.	—	—	—	—	2^M	—	—	—	2^M	1^M	0.03^M
C2000	Bal.	23	16	3^M	—	1.6	—	2^M	0.5^M	—	0.5^M	—	—	0.08^M	0.01^M
C22	Bal.	22	13	3	3	0.5^M	—	2.5^M	0.5^M	—	—	0.35^M	—	0.08^M	0.015^M
C276	Bal.	16	16	5	4	0.5^M	—	2.5^M	1^M	—	—	0.35^M	—	0.08^M	0.01^M
625	Bal.	21	9	5^M	—	0.5^M	3.7	1^M	0.5^M	0.4^M	0.4^M	—	—	0.5^M	0.1^M

(A) ^{M} indicates an alloying element's maximum percentage by weight. * also contains tantalum.

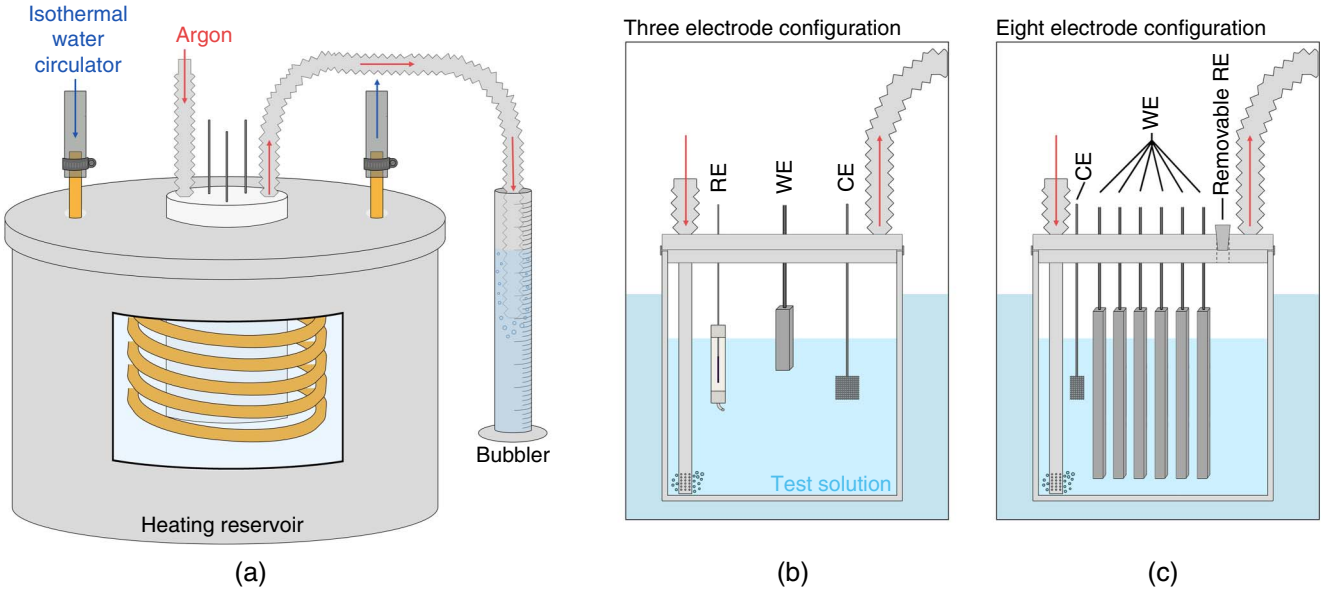

FIGURE 1. *Schematic illustration of the full assembled PTFE electrochemical cell placed within the heating reservoir (a), with a cutaway showing the placement of cell and heat-exchanger coils. Insets show a cross section of the electrochemical cell in the three-electrode (b) and eight-electrode (c) configurations.*

assembled electrochemical cell, clamp, and heating reservoir are illustrated in Figure 1(a). Once assembled, the electrochemical cell was secured in the heating reservoir, and an initial 30-min heating/purging period was observed. During this time, the temperature of the heating reservoir was increased to the desired set point, and the experimental solution was sparged vigorously with Ar gas. After this initial period, the rate of Ar sparging was lowered, and the experiment was performed.

Corrosion behavior was studied both at open-circuit (i.e., the corrosion potential [E_{CORR}] was monitored as a function of time) and during dynamic and static polarization experiments. In studies investigating behavior at E_{CORR}, the electrochemical cell was outfitted with one coupon of each of the six alloys, serving as WEs. Measurements began 24 h after the cell and electrodes were installed into the heating reservoir. Measurements, taken at 24-h intervals, included E_{CORR} and linear polarization resistance (LPR) measurements. Behavior was studied for a total of 360 h (15 d). LPR measurements were performed by polarizing each WE ± 15 mV (vs. E_{CORR}) at a scan rate of 10 mV/min. Polarization resistance (R_P) values were then extracted from the slope of the current density response (Δi) to potential changes (ΔE). Between measurements, the RE was removed from the cell to avoid long-term drift.

All dynamic and static polarizations began with a 90-min E_{CORR} measurement followed by a 30-min potentiostatic hold (–0.500 $V_{Ag/AgCl}$) as a cathodic pretreatment to ensure a reproducible surface between repeat experiments. Upon completion of the cathodic treatment, either a dynamic or a static polarization experiment was performed. In potentiodynamic experiments, the potential was scanned in the positive direction from the hold potential at a scan rate of 10 mV/min until the resultant current reached the chosen anodic limit (10 mA). In potentiostatic experiments, immediately following the potential hold, the electrode was polarized to the desired potential in a single step. Following the completion of all experiments, the temperature of the electrochemical cell was checked to make sure it had remained at the set temperature. Experimental coupons were stored in an Innovative Technology PureLab HE† Ar-filled glovebox during the period between completion of the electrochemical experiment and commencement of the surface analysis. All electrochemical measurements were repeated a minimum of two times.

2.3 | Surface Analysis

X-ray photoelectron spectroscopy (XPS) analyses were performed on the Kratos AXIS Nova† and Kratos AXIS Supra† spectrometers located at Surface Science Western. In all spectra, an Al Kα (1,486.7 eV) monochromatic x-ray source was used. The Au $4f_{7/2}$ metallic binding energy (83.95 eV) was used as a reference point for calibration of the instrument work function. Both survey and high-resolution spectra were collected on all coupons. For Ni-based coupons, the Ni 2p, Cr 2p, Mo 3d, Cu 2p, O 1s, S 2p, and C 1s were collected. For Fe-based coupons, the Fe 2p, Cr 2p, Mo 3d, O 1s, S 2p, and C 1s were collected. CasaXPS† software (v.2.3.19) was used to process spectra. All spectra were charge-corrected by adjusting the C-C binding energy in the high-resolution C 1s spectrum (284.8 eV). Fitting parameters used in the deconvolution of high-resolution spectra were taken from the work of Biesinger, et al. (Ni,[15-16] Cr,[16-17] and Fe[16]) and Spevack, et al. (Mo[18]).

2.4 | Solution Analysis

Solution samples collected at the completion of potentiostatic polarization experiments were analyzed using inductively coupled plasma mass spectrometry (ICP-MS) at the Biotron Research Facility (Western University). Samples were diluted, filtered (0.45 µm), and then analyzed using an Agilent 7700x† ICP-MS. The instrument was calibrated using aqueous standards in 2% HNO_3.

RESULTS AND DISCUSSION

3.1 | Behavior at the Corrosion Potential

The behavior under natural corrosion conditions was studied in the base electrolyte, 0.1 M Na_2SO_4, as well as in 0.1 M

Na_2SO_4 + 5,000 ppm F^- + 1,000 ppm Cl^-. In both solutions, values of E_{CORR} and R_P were measured at 1-d intervals for a total of 15 d. Considering the behavior of all six alloys in both solutions, only minor differences were found. In both solutions, values of E_{CORR} were found to stabilize within the range of approximately −0.2 V to −0.32 V and showed only minor fluctuations between measurements, as shown in Figure 2(a). Similarly, values of R_P were found to approach an apparent steady-state condition, as shown in Figure 2(b). All alloys exhibited excellent corrosion performance in both solutions, as suggested by the relative stability of E_{CORR} values and measured R_P values in the range of 10^6 Ω·cm^2 to 10^7 Ω·cm^2. A few general points are, however, worth mentioning.

Comparing the Ni- and Fe-based alloys studied here, the Ni-based alloys experience only slightly better corrosion resistance under natural corrosion conditions. As shown in Figure 2(b), this was true for both solutions examined here, i.e., with or without F^-/Cl^-. Both stainless steel alloys, SS316L and SS2205, were found to exhibit R_P values lower than those measured on Ni-based alloys at the completion of the 15-d period. Among Ni-based alloys, C2000 was found to have the highest R_P values in both solutions. Nonetheless, all measurements made under natural corrosion conditions suggest that the behavior of these alloys was consistent with strong passivity, regardless of the solution composition.[19]

While electrochemical studies showed that the alloys behaved comparably in both 0.1 M Na_2SO_4 and 0.1 M Na_2SO_4 + 5,000 ppm F^- + 1,000 ppm Cl^-, subtle differences in surface composition were identified by XPS. Table 2 summarizes the normalized surface compositions for coupons following the 15-d exposure experiment. For all alloys, a substantial decrease in Cr content was observed following exposure to the F^-/Cl^--containing solution, which was not the case for the same materials after exposure to only the 0.1 M Na_2SO_4 solution. These changes were facilitated by an interaction of Cr with one or both of these anions and will be discussed in greater detail in the *Potentiodynamic Polarization Behavior* and *Potentiostatic Polarization Behavior* sections.

It is worth mentioning that, while SS2205 and SS316L contain alloyed Ni in the amounts of 6.5 wt% and 14 wt%, respectively, the quantification of Ni by XPS was made difficult by a series of peak overlaps. More specifically, the series of Auger signals (LMM) produced by Fe overwhelmed the relatively weak signal produced by the alloyed Ni (2p). Similarly, peak overlaps complicated the quantification of Fe in the Ni-based alloys, even though they contain alloyed Fe ranging from 3 wt% to 5 wt%. In this case, the Auger signals (LMM) produced by Ni overwhelmed the photoelectron signal produced by alloyed Fe (2p). While not considered in the quantification, it is expected that Ni and Fe represent a small portion of oxidized surface species on Fe- and Ni-based alloys, respectively.[20-21] Also, the element Nb, despite making up 3.7 wt% of Alloy 625, was not detected by XPS at the end of these exposure tests.

3.2 | Potentiodynamic Polarization Behavior

Polarization curves recorded both in the base electrolyte and in solutions containing various F^- and Cl^- concentrations are shown in Figures 3(a) through (d). In all solutions, the current-potential relationship was consistent with the formation of a protective oxide film, in agreement with the observations made at E_{CORR} (discussed in the *Behavior at the Corrosion Potential* section). Current densities measured in the passive region were ≤ 10^{-6} A/cm^2, as is typical for Cr-containing alloys.[21] Formation of a passive film was observed in all solutions, regardless of the anion concentration. Passive films did not appear to be susceptible to localized breakdown, which would be indicated by momentary increases in current density. However, as applied potentials were increased, current densities were found to increase, indicating the onset of transpassive film breakdown. Here, the electrochemical conversion of Cr(III) into soluble Cr(VI) species, Equation (1), resulted in damage to the passive film. This process, commonly referred to as transpassive dissolution, has been extensively studied on Ni-, Fe-, and Co-based alloys.[1,21-24]

$$CrO_4^{2-} + 8H^+ + 3e^- \rightleftharpoons Cr^{3+} + 4H_2O \quad (1)$$

Prior to the onset of transpassive dissolution, all alloys displayed a small feature within the passive region. This feature, which occurred at approximately 0.100 V, appeared as a slight increase in current density. However, in all cases, the current density returned to the original passive current density, indicating the re-establishment of passivity. This feature has not been reported in the literature, and the cause is currently

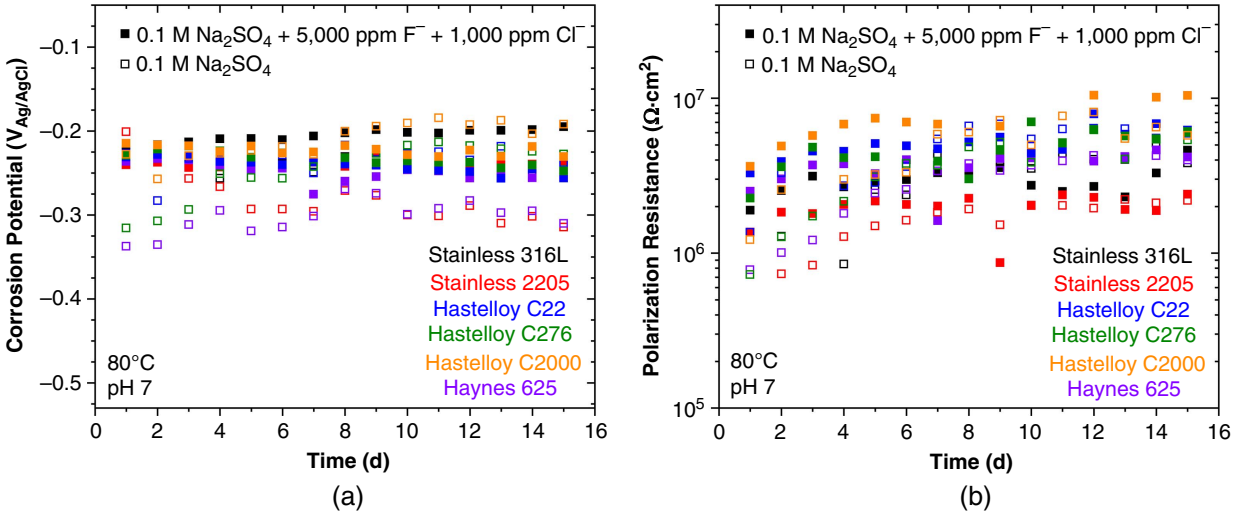

FIGURE 2. *Comparison of measured E_{CORR} (a) and R_P (b) values over a 15-d period in the absence of F^- or Cl^- (▫) and with the addition of 5,000 ppm F^- and 1,000 ppm Cl^- (▪).*

Table 2. *Normalized Surface Compositions (at%), Determined by XPS, of Alloys After Exposure to 0.1 M Na_2SO_4 or 0.1 M Na_2SO_4 + 5,000 ppm F^- + 1,000 ppm Cl^- (pH 7)*

Alloy	Solution	Ni	Fe	Cr	Mo	Cu
SS2205	0.1 M Na_2SO_4	—	30.6	64.8	4.6	—
	0.1 M Na_2SO_4 + 5,000 ppm F^- + 1,000 ppm Cl^-	—	54.8	43.1	2.1	—
SS316L	0.1 M Na_2SO_4	—	44.9	53.0	2.1	—
	0.1 M Na_2SO_4 + 5,000 ppm F^- + 1,000 ppm Cl^-	—	73.5	25.1	1.3	—
C2000	0.1 M Na_2SO_4	35.8	—	50.7	9.0	4.5
	0.1 M Na_2SO_4 + 5,000 ppm F^- + 1,000 ppm Cl^-	72.0	—	22.6	3.2	2.2
625	0.1 M Na_2SO_4	24.3	—	68.5	7.2	—
	0.1 M Na_2SO_4 + 5,000 ppm F^- + 1,000 ppm Cl^-	71.3	—	25.5	3.2	—
C22	0.1 M Na_2SO_4	37.5	—	55.7	6.8	—
	0.1 M Na_2SO_4 + 5,000 ppm F^- + 1,000 ppm Cl^-	74.4	—	22.2	3.3	—
C276	0.1 M Na_2SO_4	26.5	—	65.1	8.4	—
	0.1 M Na_2SO_4 + 5,000 ppm F^- + 1,000 ppm Cl^-	79.2	—	17.7	3.1	—

unknown. Nevertheless, the significance of this behavior, in relation to corrosion, appears to be minor.

As the applied potential increased beyond the onset of transpassivity, current densities rapidly increased on Ni-based alloys due to continued metal dissolution following film breakdown. For Cr-containing alloys, the rates of dissolution following transpassive film breakdown have been shown to be increased by increases in Mo content and suppressed by increases in Fe content.[25-27] This is consistent with data presented here, which show a higher rate of increase of the current density with potential for Alloy C2000 (16 wt% Mo) than for Alloy 625 (9 wt% Mo), as shown in Figures 3(a) through (c). This increase has been tentatively assigned to an ill-defined catalytic effect of Mo on transpassive dissolution.[25-27] Fe-based alloys were found to have a secondary passive region at applied potentials higher than the onset of electrochemical conversion of Cr(III) to Cr(VI). While current densities increased at the onset of the Cr(III) oxidation, a second current plateau was observed for the Fe-based alloys. This was the result of corrosion inhibition by Fe(III) oxides formed at the surface.[19] Within this secondary passive region, current densities were found to be two to three times higher than those recorded in the primary passive region. The secondary passive region was comparable on SS316L and SS2205, and it persisted until approximately 0.900 V.

While comparing Figures 3(a) and (b) illustrates that the addition of 1,000 ppm Cl^- resulted in no visible change to the polarization behavior relative to the base electrolyte, the addition of F^- ions was found to modify the current-potential response. The current-potential responses of alloys exposed to 1,000 ppm F^- and 5,000 ppm F^- (with 1,000 ppm Cl^-) are displayed in Figures 3(c) and (d), respectively. F^- ions mainly influenced the transpassive behavior; a direct comparison of the transpassive behavior recorded in the different experimental solutions is given in Figure 4 for (a) Alloy C22 and (b) SS2205. As indicated by the markings along the lower ordinate axis, the introduction of F^- ion resulted in a decrease in the onset potential of Cr(III) oxidation. In comparison to solutions without F^-, the breakdown of the passive region was decreased by approximately 0.100 V in the presence of F^- ions.

Furthermore, considering the secondary passive region present on SS2205 and SS316L (Figure 3[c]), the introduction of 1,000 ppm F^- resulted in a loss of stability in the secondary passive region and an eventual breakdown at approximately 0.65 V. In solutions containing 5,000 ppm F^- and 1,000 ppm Cl^-, while the breakdown of the secondary passive layer was observed, a subsequent decrease in current density suggested that a film repair/deposition process occurred as the potential was increased further, as shown in both Figures 3(d) and 4(b). While an attempt to repassivate the surface is apparent, fluctuations in current density observed beyond the breakdown potential (i.e., for potentials >0.6 V) indicate that this "reformed" film is only partially stable and, hence, susceptible to further breakdown. In general, the presence of F^- has been shown to lead to enhanced reactivity at Fe-based alloy surfaces through the formation of soluble Fe-F species.[28-31]

A series of potentiodynamic experiments were also conducted at pH 5 and pH 9 for both the base electrolyte and the electrolyte-containing 0.1 M Na_2SO_4 + 5,000 ppm F^- + 1,000 ppm Cl^-. In general, the polarization behavior, including the primary and secondary passive regions, as well as changes in transpassivity, were similar to those found in pH 7 solutions (Figure 3) and are therefore not shown. In the pH range 5 to 9, all alloys maintained current densities less than 10^{-6} A/cm^2 in the primary passive region, consistent with the presence of a Cr(III)-rich oxide layer.[19] Based on the solubility data for Cr species, a decrease in pH to values less than approximately 4 would be required to challenge this passivity.[19,32] Wang, et al., studied the behavior of SS316 in H_2SO_4 (pH 1) with and without Cl^- and F^-.[2] Under their conditions, active behavior was observed at low potentials, with an active-to-passive transition and, hence, the establishment of passivity occurring only as the potential was increased. Currents in the active region were found to be increased by F^- but not by Cl^-. In addition, Wang, et al., did not observe a secondary passive region, which is not surprising at such low pH, where the solubility of Fe(III) species would be considerably higher than in the experiments presented here.[32]

Under the examined conditions, the most significant impact of F^- ions appears to be an early onset of transpassive dissolution. The average (n = 2–4) transpassive potentials found in the various solutions at pH 7, and the influence of changes in pH in the range 5 to 9 are depicted in Figures 5(a) and (b), respectively. At pH 7, in solutions containing F^- ion,

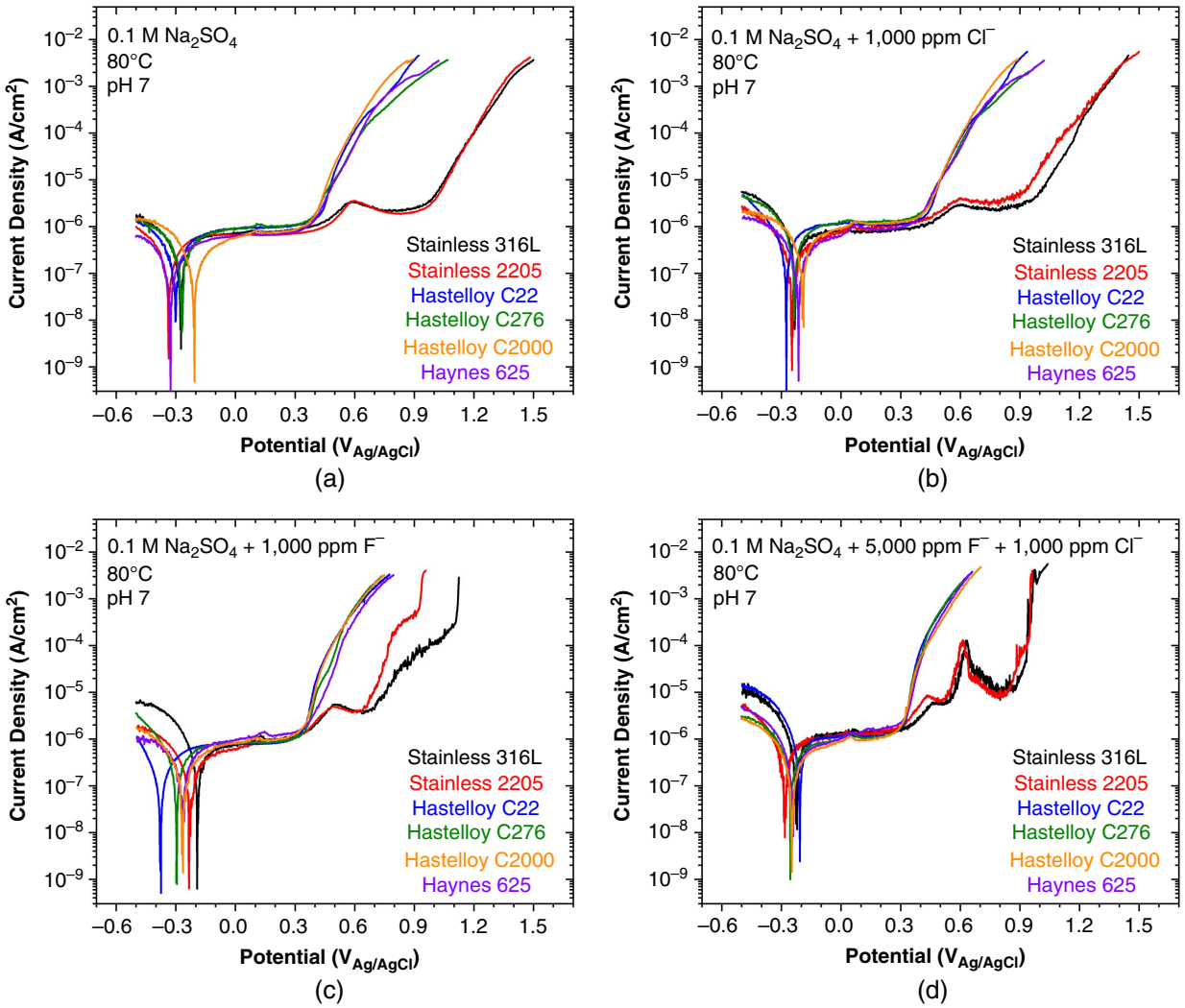

FIGURE 3. *Potentiodynamic polarization behavior of alloys in 0.1 M Na_2SO_4 solution in the absence of F^- or Cl^- (a), with 1,000 ppm Cl^- (b), with 1,000 ppm F^- (c), and with 5,000 ppm F^- + 1,000 ppm Cl^- (d).*

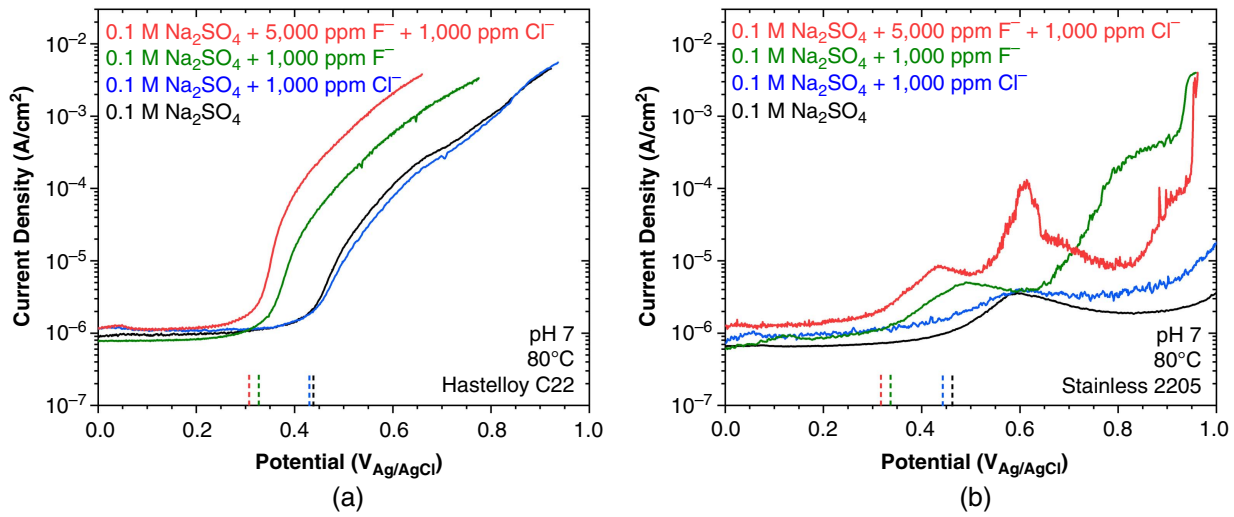

FIGURE 4. *Comparison of transpassive regions for Alloy C22 (a) and SS2205 (b) exposed to the various solutions indicated in the legend. Extracted transpassive onset potentials are indicated by the markings along the lower ordinate axis.*

shown as green and red in Figure 3(a), the alloys were found to undergo transpassive dissolution at lower applied potentials than in solutions without F^- ions. On average, the onset of transpassivity was found to decrease by approximately 0.1 V with the addition of F^-, which is believed to be the result of an interaction of F^- with the Cr(III)-rich film, resulting in the formation of CrF_3 species,[2,29,33] as shown by Equation (2). These interactions have been shown to result in the conversion of the insoluble Cr_2O_3 film into the semisoluble CrF_3 species, ultimately leading to the degradation of the protective passive film. Similar behavior has been found on other metals including Fe, Ni, Ti, Al, and Sn.[34-38]

$$Cr_2O_3 + 6H^+ + 6F^- \rightleftharpoons 2CrF_3 + 3H_2O \quad (2)$$

A comparison of the average transpassive potentials exhibited by alloys immersed in the base electrolyte, 0.1 M Na_2SO_4, and the most ionically concentrated solution, 0.1 M Na_2SO_4 + 5,000 ppm F^- + 1,000 ppm Cl^-, at the three pH values investigated (5, 7, and 9) is shown in Figure 5(b). Overall, during immersion in the base electrolyte, alloys exhibited decreasing transpassive onset potentials as solutions became more alkaline. This was attributed to the pH dependence of the equilibrium potential for the redox conversion of Cr(III) to Cr(VI),[19] per Equation (1). At pH 9, the presence of F^- exerted no influence on the transpassive potential, but its influence increased markedly as the pH was decreased. While the influence of F^- ions on the onset of transpassivity was apparent for pH 5 and pH 7, changes were less severe at pH 9. It is likely that the decreasing solubility of Cr(III) species across the range of pH values (5, 7, and 9) limits the formation of these Cr-F species.[19]

3.3 | Potentiostatic Polarization Behavior

Potentiostatic polarization experiments were conducted on two alloys, SS2205 and C2000. These alloys were selected based on their extensive use in the petrochemical industry (SS2205) and for literature reports regarding the beneficial effects of Cu addition on the corrosion behavior in F^--containing solutions (C2000). Changes in surface composition and dissolved metal concentrations were monitored at the conclusion of polarization measurements by XPS and ICP-MS, respectively.

Current densities recorded at applied potentials of −0.100 V, 0 V, 0.100 V, 0.200 V, and 0.300 V in solution containing 5,000 ppm F^- and 1,000 ppm Cl^- (pH 5) are shown in Figures 6 and 7 for C2000 and SS2205, respectively. For clarity, data are presented on both semi-log (a) and log-log (b) axes. At the lower applied potentials, e.g., −0.100 V, 0 V, and 0.100 V, observations were similar for C2000 and SS2205. Plotting these data on log-log axes, as shown in Figures 6(b) and 7(b), demonstrates that the current densities decreased with time in an approximately linear fashion for the entire 8-h period. These decreases in current density are consistent with the anodic formation of a passive oxide film. Unlike SS2205, at an applied potential of 0.100 V, C2000 achieved a steady-state condition for t > 2 h, indicating that the film growth process was accompanied by a dissolution process (steady state is achieved once the rates of film growth and film dissolution become equal).

At higher potentials, e.g., 0.200 V and 0.300 V, both C2000 and SS2205 showed current densities decreasing with time. However, current densities were higher as the applied potential increased. Although current densities initially showed a decreasing trend, sudden increases in current densities were observed, indicating a breakdown of the passive oxide formed at shorter times. Current densities were considerably lower, by almost two orders of magnitude, on the Fe-based alloy (Figure 7) than on the Ni-based alloy (Figure 6). Considering the dynamic polarization behavior, as shown in Figure 3, the protection provided by Fe(III) oxides is apparent; lower measured current densities on SS2205 are explained by the higher stability of Fe(III) oxide at higher potentials.[19]

Current transients recorded on C2000 and SS2205 at 0.200 V and 0.300 V in the base electrolyte solution were compared to those insolution containing F^-/Cl^- in Figures 8 and 9, respectively. First, considering the transients recorded at the lower applied potential, 0.200 V, films grew for a minimum of 9,000 s and 2,000 s on C2000 and SS2205, respectively. Beyond this period, differences were observed in the corrosion behavior between alloys exposed to solutions containing F^-/Cl^- and those exposed to the base electrolyte only. In the case of C2000, exposed to the base electrolyte (Figure 8), film growth continued until a steady state was eventually attained. In the solution containing F^-/Cl^-, film growth continued until currents began to increase at t > 9,000 s, suggesting a film breakdown. In the case of SS2205 (Figure 9), following the initial

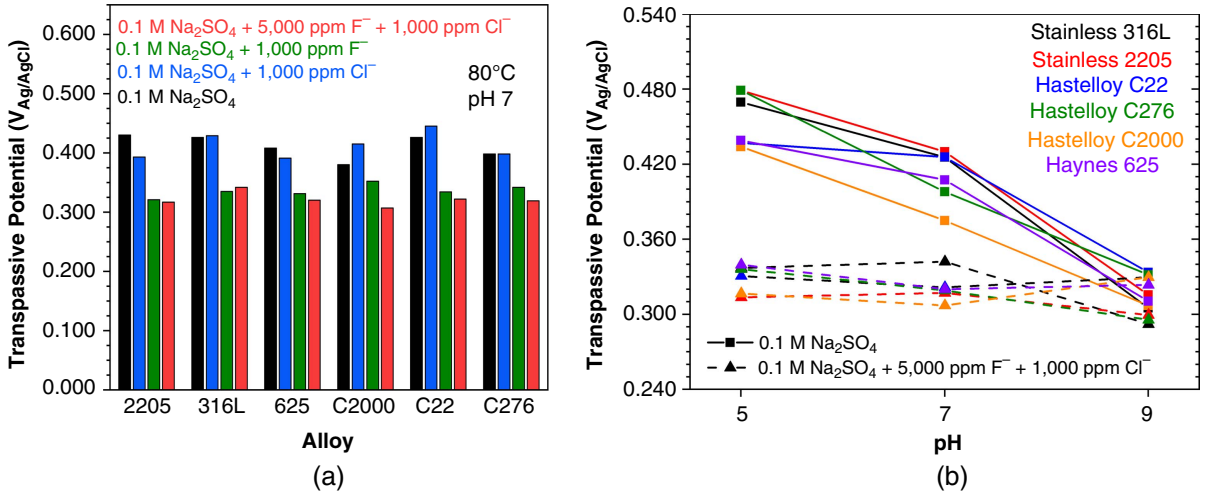

FIGURE 5. *Average (n = 2–4) transpassive potentials of alloys in different solutions at pH 7 (a) and a comparison of the transpassive potentials of alloys in the 0.1 M Na_2SO_4 and 0.1 M Na_2SO_4 + 5,000 ppm F^- + 1,000 ppm Cl^-solutions (b) as a function of pH.*

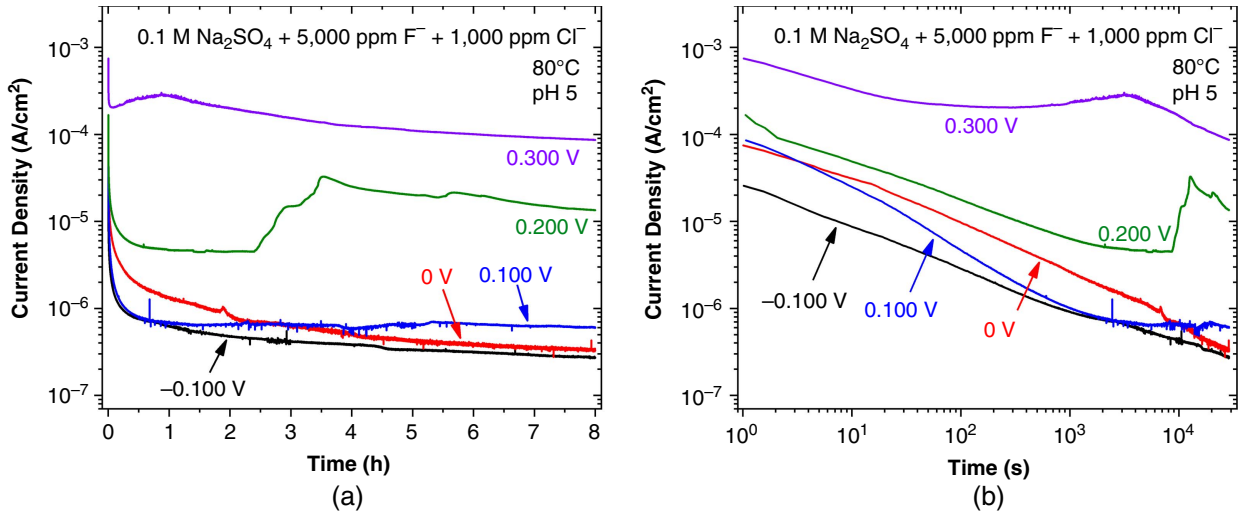

FIGURE 6. *Current-time response for C2000 electrodes polarized at −0.100 V, 0 V, 0.100 V, 0.200 V, and 0.300 V while immersed in 0.1 M Na_2SO_4 + 5,000 ppm F^- + 1,000 ppm Cl^- solution. The same data are presented as log(i)-time (a) and log(i)-log(t) (b) plots.*

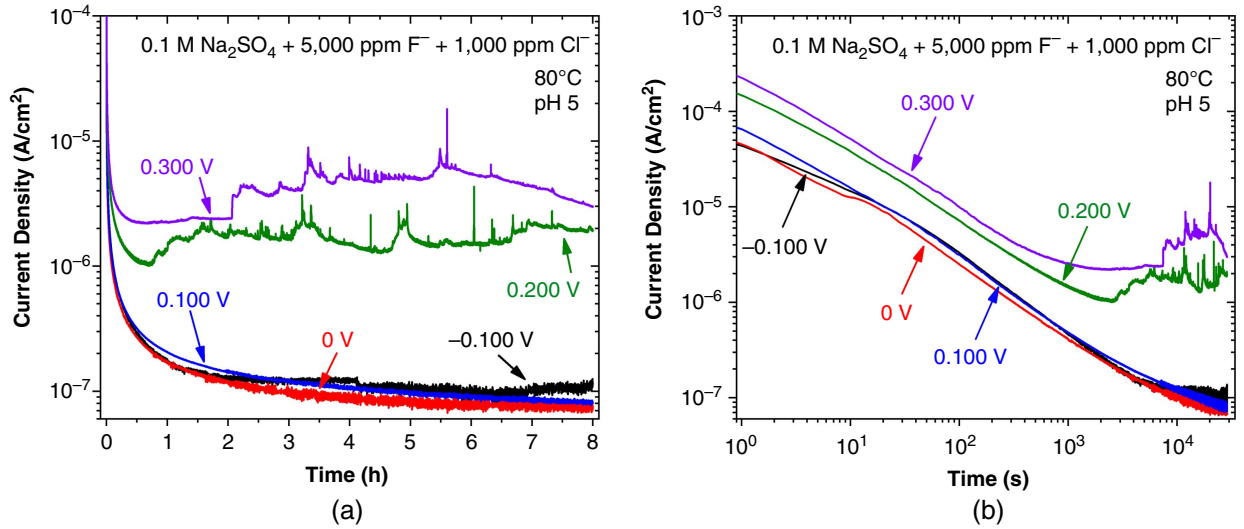

FIGURE 7. *Current-time response for SS2205 coupons polarized at −0.100 V, 0 V, 0.100 V, 0.200 V, and 0.300 V while immersed in 0.1 M Na_2SO_4 + 5,000 ppm F^- + 1,000 ppm Cl^- solution. The same data are presented as log(i)-time (a) and log(i)-log(t) (b) plots.*

period of film growth, minor current transients became apparent in the base electrolyte. All transients returned to the background current values, suggesting repassivation. Despite these metastable events, film growth continued, as suggested by further decreases in current densities over time. In the F^-/Cl^--containing solution, breakdown behavior was more frequent than in the base electrolyte. In solutions containing F^-/Cl^-, an increase in background current density occurred at t > 3,000 s, suggesting the presence of competing film formation and dissolution processes.

At the highest applied potential, 0.300 V, differences between the current transients recorded on materials exposed to the F^-/Cl^--containing solutions and those exposed to the base electrolyte were again apparent. While an initial film growth process was observed on C2000 in both solutions, current densities measured in the F^-/Cl^--containing solution were approximately one order of magnitude higher than those measured in the base electrolyte, as shown in Figure 8.

Furthermore, in both solutions, the presence of current fluctuations suggests the general instability of the surface oxide, which is not unexpected, due to the onset of transpassive dissolution at higher applied potentials. In the case of SS2205, current densities measured during the film growth were similar in both the base electrolyte and in the solution containing F^-/Cl^-, per Figure 9. At t > 4,000 s, passive film breakdown behavior became apparent in both the base electrolyte and the F^-/Cl^--containing solution. However, the current fluctuations were more pronounced when F^- was present.

Solution analysis, obtained by ICP-MS, confirmed metal ion release at the onset of film breakdown at an applied potential of 0.300 V in solutions containing F^-/Cl^-. The concentrations of dissolved Ni and Fe, the alloy matrix elements for C2000 and SS2205, respectively, are shown as a function of the applied potential in Figure 10. For both C2000 and SS2205, concentrations of dissolved Ni or Fe, respectively, remained below limits of detection (indicated as a dotted line) for applied potentials

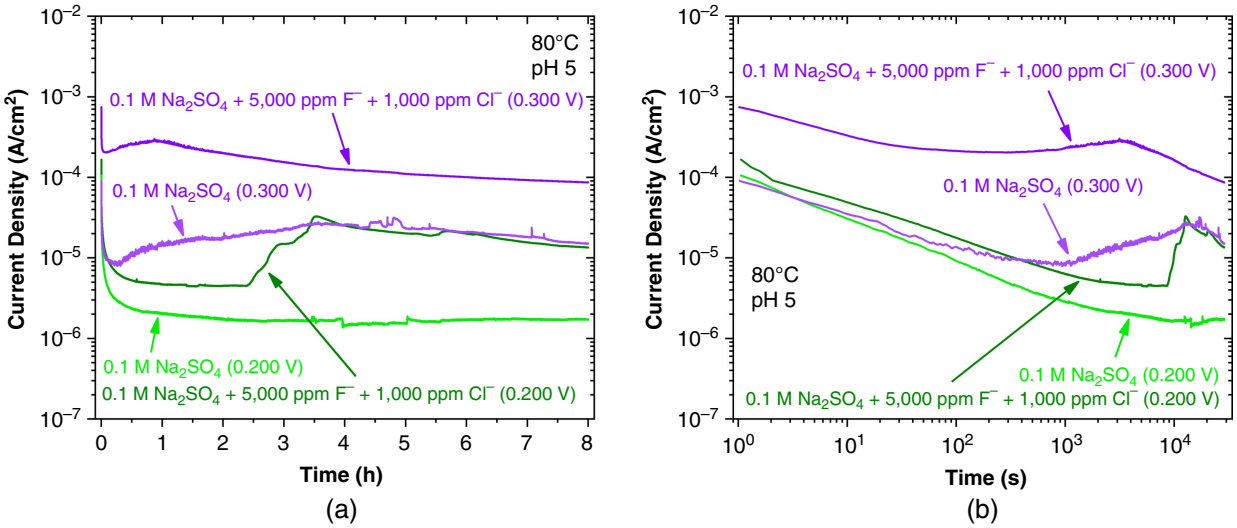

FIGURE 8. *The effect of F^- and Cl^- addition to the base electrolyte (0.1 M Na_2SO_4) is compared for applied potentials of 0.200 V and 0.300 V for Alloy C2000. Presented as log(i)-time (a) and log(i)-log(t) (b) plots.*

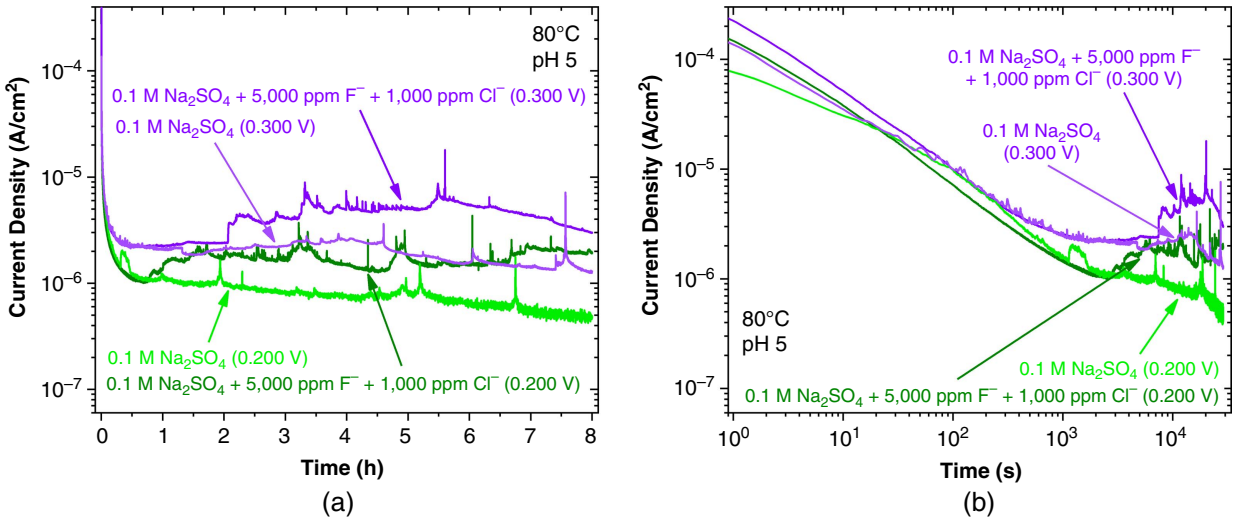

FIGURE 9. *The effect of F^- and Cl^- addition to the base electrolyte (0.1 M Na_2SO_4) is compared for applied potentials of 0.200 V and 0.300 V for SS2205. Presented as log(i)-time (a) and log(i)-log(t) (b) plots.*

≤ 0.200 V. The ability of Ni and Fe to remain below detection limits, despite the 8-h polarization, is evidence of the protective nature of the oxide films formed at these potentials. At an applied potential of 0.300 V, passivity gave way to transpassive behavior, as confirmed by the sudden increase in Ni and Fe concentrations. This is especially true for (a) C2000, where Ni suddenly became detectable at levels approximately 12 times the limit of detection, and (b) SS2205, where Fe became detectable only at the applied potential of 0.300 V. Comparing the concentrations of dissolved metal ions from C2000 and SS2205, one can note that concentrations of dissolved Fe from SS2205 were significantly lower than the levels of Ni released from C2000. This agreed with the measurement of lower current densities on SS2205 than on C2000.

Alloy surface compositions following potentiostatic experiments in solutions containing 5,000 ppm F^- and 1,000 ppm Cl^- were investigated by XPS. Surface compositions obtained by the quantification of survey spectra are summarized in Tables 3 and 4 for C2000 and SS2205, respectively. As expected, the surface composition within the passive region was dominated by Cr on C2000 and by both Cr and Fe on SS2205. At 0.300 V, i.e., with the onset of transpassivity, the apparent concentrations of the individual metals decreased. This mainly reflects the thickening of the oxide film, such that XPS analysis, which determines a weighted average composition of the outermost several nanometers of the surface, detects less of the underlying metal and more oxygen, resulting in what seems like dilution of the metal concentration. To a lesser extent, the formation of higher oxidation states of Cr, Fe, and Mo at these potentials, and their subsequent hydrolysis, also contribute to this dilution effect.

Although both F^- and Cl^- were present in solution, only F was detected on the surface following the potentiostatic polarization experiments. This suggests that F^- may be incorporated into the growing oxide, a feature that would explain the breakdown of the oxide at lower potentials when F^- is

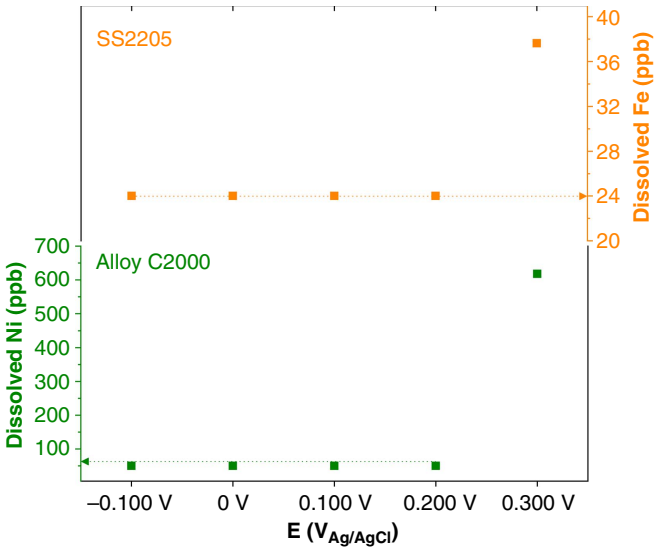

FIGURE 10. *Concentrations of dissolved alloy matrix elements, determined by ICP-MS, as a function of applied potential. Solution samples were taken at the completion of potentiostatic polarization experiments on SS2205 and C2000 in 0.1 M Na_2SO_4 + 5,000 ppm F^- + 1,000 ppm Cl^- (pH 5 and 80°C). Values are expressed in µg/L (ppb).*

present. The incorporation of F into surface oxides has been observed in acidic F^--containing media.[39] Here, the tendency of F to remain in the surface appears to increase with increasing potentials. At high potentials, the small decrease in the concentration of F can be attributed to the sharp increase in O content achieved in this region.

Two additional features are worth noting:

1. The absence of a signal for Cl^- indicates that it is not incorporated into the oxide, at least not in detectable concentrations. This is consistent with the results in Figure 2, which show that the addition of Cl^- to the base electrolyte (at pH 7) had little influence on the potentiodynamic polarization curve.
2. No signal was observed for Cu on Alloy C2000, indicating that no segregation of Cu to the alloy/solution interface took place during anodic oxidation. Some studies in concentrated HF have shown Cu segregation to the interface,[7] which could indicate that this process does not take place in the pH range 5 to 9.

Normalized surface compositions, incorporating chemical state information, are shown in Figures 11(a) and (b) for C2000 and SS2205, respectively. Here, the normalized surface composition obtained from survey spectra was combined with the chemical state information provided by deconvoluting high-resolution spectra. In the passive region (−0.100 V to 0.200 V), surfaces of both C2000 and SS2205 were dominated by oxidized Cr/Fe species, consistent with the presence of the barrier layer associated with passivity.[4,21] For both alloys, signals representing metallic components demonstrate the passive oxide to be relatively thin within the passive region and to thicken once the potential was increased into the transpassive region (0.300 V). In a previous study of electrochemically grown films on C2000, Zhang, et al., demonstrated the tendency for the oxide thickness to increase near the onset of transpassive dissolution.[21] Although not shown here, the $Ni(OH)_2$ content of the film on C2000, a signature for its tendency to dissolve, becomes noticeable for potentials between 0 V and 0.100 V.[21]

Following the polarization experiments, the electrode surfaces were examined by scanning electron microscopy to determine changes in surface morphology resulting from dissolution during the polarizations. In all cases, the degree of dissolution attack was too small to observe, as evidenced by the retention of grinding lines generated by surface preparation procedures.

Table 3. *Surface Composition (at%), Determined by XPS, of C2000 Coupons Immersed in a Solution Containing 0.1 M Na_2SO_4 + 5,000 ppm F^- + 1,000 ppm Cl^- (pH 5 and 80°C) and Polarized at the Indicated Potential for 8 h*[(A)]

	Ni	Cr	Mo	O	F
−0.100 V	2.9	14.4	3.7	77.9	1.1
0 V	3.7	15.3	4.3	75.2	1.5
0.100 V	5.4	15.3	3.9	72.4	3.1
0.200 V	3.0	15.8	4.1	74.7	2.5
0.300 V	1.3	11.5	0.3	84.9	2.0

[(A)] The contribution of the C 1s signal has been factored out of the reported data.

Table 4. *Surface Composition (at%), Determined by XPS, of SS2205 Coupons Immersed in a Solution Containing 0.1 M Na_2SO_4 + 5,000 ppm F^- + 1,000 ppm Cl^- (pH 5 and 80°C) and Polarized at the Indicated Potential for 8 h*[(A)]

	Fe	Cr	Mo	O	F
−0.100 V	23.1	12.4	0.8	62.9	0.8
0 V	27.7	8.4	0.5	63.0	0.4
0.100 V	21.0	14.9	0.7	62.4	0.9
0.200 V	16.0	6.4	0.8	76.2	0.6
0.300 V	20.8	2.0	0.1	75.7	1.3

[(A)] The contribution of the C 1s signal has been factored out of the reported data.

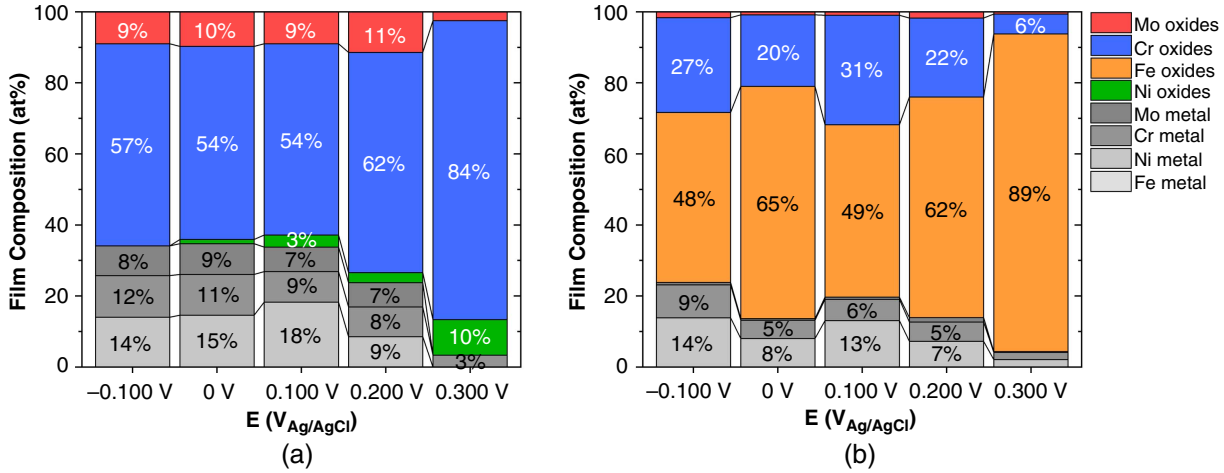

FIGURE 11. *Normalized surface composition (at%), determined by XPS, of C2000 (a) and SS2205 (b) showing major alloying elements (Ni or Fe, Cr, Mo) and their compounds following potentiostatic polarization. Components contributing ≤ 2 at% are not labeled.*

CONCLUSIONS

➢ The ability of fluoride ions to decrease the onset potential for transpassive breakdown on Cr-containing alloys, and to challenge the secondary passive window of Fe-based alloys, has been documented. Dynamic polarization experiments demonstrated that onset potentials for the transpassive region were decreased by approximately 0.100 V in the presence of fluoride ions. This was particularly apparent in slightly acidic solutions (pH 5) and becomes less severe at higher pH. Potentiostatic polarization experiments support observations regarding the ability of fluoride ions to promote transpassive dissolution.

➢ Findings suggest that Fe-based alloys experience lower corrosion rates at the onset of transpassive dissolution than do Ni-based alloys. This was attributed to the protectiveness and low solubility of oxidized Fe species within the surface film at potentials beyond the electrochemical conversion of Cr(III) to Cr(VI).

➢ While values of E_{CORR} recorded under the conditions employed here are less than those required for transpassive film breakdown, the role of fluoride ions is expected to become important in the presence of oxidizing impurities commonly found in industrial processes.

ACKNOWLEDGMENTS

This work would not have been possible without support from the Imperial Oil (Sarnia, ON) University Research Award (URA). Author J.D.H. would like to thank Dr. Dmitrij Zagidulin for his many ideas and support during the execution of these experiments. Author J.D.H. also acknowledges the support the NSERC CGS-D scholarship. Lastly, Frank Van Sas and Brian Dalrymple (Machine Shop, Dept. of Physics, Western University) are credited for their excellent work in the realization of the PTFE electrochemical cell.

References

1. S. Pahlavan, S. Moazen, I. Taji, K. Saffar, M. Hamrah, M.H. Moayed, S. Mollazadeh Beidokhti, *Corros. Sci.* 112 (2016): p. 233-240.
2. Z.B. Wang, H.X. Hu, Y.G. Zheng, *Corros. Sci.* 130 (2018): p. 203-217.
3. H.S. Klapper, N.S. Zadorozne, R.B. Rebak, *Acta Metall. Sin.* 30 (2017): p. 296-305.
4. Z. Wang, A. Seyeux, S. Zanna, V. Maurice, P. Marcus, *Electrochim. Acta* 329 (2020): p. 135159.
5. NACE Technical Committee, "Materials for Storing and Handling Commercial Grades of Aqueous Hydrofluoric Acid and Anhydrous Hydrogen Fluoride," NACE Technical Committee Report (5A171), NACE International, Houston, TX, 2007.
6. Y. Li, X. Fan, N. Tang, H. Bian, Y. Hou, Y. Koizumi, A. Chiba, *Corros. Sci.* 78 (2014): p. 101-110.
7. Y. Li, X. Xu, Y. Hou, C. Zhang, F. Wang, K. Omura, Y. Koizumi, A. Chiba, *Corros. Sci.* 98 (2015): p. 119-127.
8. R.B. Rebak, J.R. Dillman, P. Crook, C.V.V. Shawber, *Mater. Corros.* 52 (2001): p. 289-297.
9. J.N. Saba, D.A. Siddiqui, L.C. Rodriguez, S. Sridhar, D.C. Rodrigues, *J. Bio. Tribo. Corros.* 3 (2017): p. 1-7.
10. J.C.M. Souza, S.L. Barbosa, E.A. Ariza, M. Henriques, W. Teughels, P. Ponthiaux, J.-P. Celis, L.A. Rocha, *Mater. Sci. Eng. C* 47 (2015): p. 384-393.
11. A.V. Rodrigues, N.T.C. Oliveira, M.L. dos Santos, A.C. Guastaldi, *J. Mater. Sci. Mater. Med.* 16 (2015): p. 1-9.
12. A. Kocijan, K.D. Merl, M. Jenko, *Corros. Sci.* 53 (2011): p. 776-783.
13. Y. Yang, L. Guo, H. Liu, *Int. J. Hydrogen Energy* 37 (2012): p. 1875-1883.
14. P. Rae, G. di Lullo, *Matrix Acid Stimulation: A Review of the State-Of-The-Art* (Richardson, TX: Society of Petroleum Engineers, 2003).
15. M.C. Biesinger, B.P. Payne, L.W.M. Lau, A. Gerson, R.C. Smart, *Surf. Interface Anal.* 41 (2009): p. 324-332.
16. M.C. Biesinger, B.P. Payne, A.P. Grosvenor, L.W.M. Lau, A.R. Gerson, R.C. Smart, *Appl. Surf. Sci.* 257 (2011): p. 2717-2730.
17. M.C. Biesinger, C. Brown, J.R. Mycroft, R.D. Davidson, N.S. McIntyre, *Surf. Interface Anal.* 36 (2004): p. 1550-1563.
18. P.A. Spevack, N.S. McIntyre, *J. Phys. Chem.* 96 (1992): p. 9029-9035.
19. M. Pourbaix, *Atlas of Electrochemical Equilibria in Aqueous Solutions* (Houston, TX: NACE, 1974).
20. X. Cheng, Z. Feng, C. Li, C. Dong, X. Li, *Electrochim. Acta* 56 (2011): p. 5860-5865.
21. X. Zhang, D. Zagidulin, D.W. Shoesmith, *Electrochim. Acta* 89 (2013): p. 814-822.
22. A.K. Mishra, D.W. Shoesmith, *Electrochim. Acta* 102 (2013): p. 328-335.
23. A.W.E. Hodgson, S. Kurz, S. Virtanen, V. Fervel, C.O.A. Olsson, S. Mischler, *Electrochim. Acta* 49 (2004): p. 2167-2178.
24. J.D. Henderson, X. Li, D.W. Shoesmith, J.J. Noël, K. Ogle, *Corros. Sci.* 147 (2019): p. 32-40.
25. M. Bojinov, G. Fabricius, T. Laitinen, T. Saario, *Electrochim. Acta* 44 (1999): p. 4331-4343.
26. M. Bojinov, I. Betova, R. Raicheff, *J. Electroanal. Chem.* 430 (1997): p. 169-178.
27. I. Betova, M. Bojinov, P. Kinnunen, T. Laitinen, P. Pohjanne, T. Saario, M. Vilpas, *J. Electrochem. Soc.* 149 (2002): p. B499-B509.

28. J.L. Galvez, J. Dufour, C. Negro, F. Lopez-Mateos, *Chem. Eng. J.* 136 (2008): p. 116-125.
29. P. Marcus, *Corrosion Mechanisms in Theory and Practice*, 3rd ed. (Boca Raton, FL: CRC Press, 2011).
30. J. Hem, *GSA Bull.* 83 (1972): p. 443-450.
31. A. Macías, M.L. Escudero, *Corros. Sci.* 36 (1994): p. 2169-2180.
32. C.F. Baes, R.E. Mesmer, *The Hydrolysis of Cations* (New York, NY: Wiley, 1976).
33. A.V. Ingle, V.S. Raja, J. Rangarajan, P. Mishra, *Fuel Cells* 19 (2019): p. 708-723.
34. J.L. Trompette, *Corros. Sci.* 94 (2015): p. 288-293.
35. S.M. Castro, M.J. Ponces, J.D. Lopes, M. Vasconcelos, M.C.F. Pollmann, *J. Dental Sci.* 10 (2015): p. 1-7.
36. H.-H. Strehblow, B. Titze, B.P. Loechel, *Corros. Sci.* 19 (1979): p. 1047-1057.
37. M. Mirjalili, M. Momeni, N. Ebrahimi, M.H. Moayed, *Mater. Sci. Eng. C* 33 (2013): p. 2084-2093.
38. B.J. Plankey, H.H. Patterson, C.S. Cronan, *Environ. Sci. Technol.* 20 (1986): p. 160-165.
39. M.C. Li, C.L. Zheng, H.C. Lin, C.N. Cao, *Brit. Corros. J.* 36 (2001): p. 179-183.